Reliability Assessment of Renewable Power Systems Considering Thermally-Induced Incidents of Large-Scale Battery Energy Storage

Siying Li, Chengjin Ye, *Member, IEEE*, Yi Ding, *Member, IEEE*, Yonghua Song, *Fellow, IEEE*, and Minglei Bao

***Abstract*—The battery energy storage system (BESS) has been envisaged as an effective solution for renewable energy accommodation in power systems. However, the residual capacity and maximum power of large-scale BESS are highly affected by thermally-induced incidents such as battery degradation and Thermal Runaway (TR) propagation. In the prior-art studies, the impacts of thermally-induced incidents on the BESS service performance have not been well modeled, resulting in relatively over-optimistic reliability estimation of power systems. In this paper, the reliability of large-scale grid-connected BESSs as well as its impacts on the overall reliability of power systems are investigated considering the battery degradation and TR propagation. To quantify the time-varying performance of the BESS, a multi-state model is constructed. The proposed model describes the aging process of batteries inside the BESS, incorporating the combined effects of sequential TR and the performance degradation of the surrounding batteries due to heat absorption. Based on the Monte Carlo method, scenarios that reflect the uncertainties of the intermittent wind generation and fluctuating loads are simulated. An optimal scheduling model is deployed, and a solution algorithm is proposed to calculate the scheduling results of the BESS in the real-time performance range subject to its thermal conditions. Case studies are conducted to validate the effectiveness of the proposed model and technique.**

***Index Terms*—Battery energy storage system, degradation, multi-state system, reliability, thermal runaway propagation.**

NOMENCLATURE

Indices and Sets

i, r	Index of batteries.
j	Index of performance levels.
b	Index of BESS.
g	Index of conventional generating units.
w	Index of wind turbines.
m	Index of electric nodes.
v	Index of iteration number.
$\Psi_{C,m}$	Set of components at node m.
$\Psi_{N,m}$	Set of nodes connected to node m.

Parameters

k_B	Boltzmann constant.
E_a^{cyc}	Activation barrier for battery cycle aging.
T_{ref}	Reference temperature.
E_i^{ini}	Initial capacity of battery cell i.
E_i^{end}	Capacity of i at the end of the battery life.
P_i^{ini}	Initial maximum power output of battery cell i.
R_i^{init}	Initial ohmic resistance of battery cell i.
$d_{i,r}$	Distance between cell i and cell r.
$\eta_{i,r}$	Efficiency of cell i in transferring heat to r.
T_{crit}	Critical temperature T_{crit} of TR.
$P_g^{\min}$ / $P_g^{\max}$	Maximum/minimum active power output of generator g at time t.
$Q_g^{\min}$ / $Q_g^{\max}$	Maximum/minimum reactive power output of generator g at time t.
$P_w^{t,avl}$	Maximum active power output of wind turbine w at time t.
RD_g / RU_g	Ramp-up/ramp-down rates of generator g at time t.
$\theta_m^{\min}$ / $\theta_m^{\max}$	Maximum/minimum phase at node m.
$V_m^{\min}$ / $V_m^{\max}$	Maximum/minimum voltage at node m.
G_{ms} / B_{ms}	Conductance/susceptance of line $m-s$.
$S_{ms}^{\max}$	Maximum apparent power of line $m-s$.
ST	Sampling number of Monte Carlo simulation.

Variables

E_i^t	Residual capacity of battery cell i at time t.
SOC_i^t	SOC of battery cell i at time t.

Manuscript received April 4, 2022; revised July 18, 2022; accepted August 18, 2022. This work was supported by the National Science Foundation for Distinguished Young Scholars of China under Grant 52125702. Paper no. TPWRS-00479-2022. (Corresponding author: *Chengjin Ye.*)

Siying Li, Chengjin Ye, Yi Ding, and Minglei Bao are with the College of Electrical Engineering, Zhejiang University, Hangzhou 310027, China (e-mail: yechenjing@zju.edu.cn).

Yonghua Song is with the State Key Laboratory of Internet of Things for Smart City, University of Macau, Macau 999078, China (e-mail: yhsong@um.edu.mo).

$H_{i,r}^t$	Heat absorbed by i from r until time t.
$P_i^{REL,t}$	Heat release rate of battery cell i at time t.
T_i^t	Temperature of battery i at time t.
$\bar{E}_b^t$	Residual capacity of BESS b at time t.
$\bar{P}_b^t$	Maximum power of BESS b at time t.
P_g^t / Q_g^t	Active/reactive power of generator g at time t.
P_w^t / Q_w^t	Active/reactive power of wind turbine w at t.
PC_m^t	Load curtailment at node m and time t.
PD_m^t / QD_m^t	Active/reactive load at node m and time t.
ΔP_w^t	Wind curtailment of wind turbine w at time t.
$x_{b,ch}^t$ / $x_{b,dis}^t$	Indicator for charging/discharging state of BESS b at t.
$P_{b,ch}^t$ / $P_{b,dis}^t$	Charging/discharging power of BESS b at t.
V_m^t / θ_m^t	Voltage/phase at node m and time t.
S_{ms}^t	Apparent power of line $m-s$ at time t.
Rel_b^t	Reliability of BESS b at time t.
$EENS_m$	Expected energy not supplied at node m.
$LOLP_m$	Loss of load probability at node m.
ΔW_t	Wind energy curtailment at time t.

I. Introduction

To combat climate change and the energy crisis, the use of renewable energy has seen rapid growth in recent years [1]. The power industry is moving towards alternative forms of energy generation such as wind power generation and photovoltaic power generation. It is predicted that renewable energy is likely to increase its share of global electricity generation from 24% in 2016 to 54% by 2030 [2]-[3]. Meanwhile, the widespread use of renewable energy poses challenges to the operation of power systems owing to its variable power generation nature. Issues including more frequent outages and larger frequency deviations mandate the exploitation of energy storage [4]-[5]. Among various energy storage technologies, battery energy storage has become a hotspot due to its advantages of fast and steady response, adaptability, and controllability [6]. According to the International Energy Agency (IEA), global installed storage capacity is forecast to expand by 56% to reach over 270 GW by 2026, and utility-scale batteries are expected to account for the majority of global storage growth, with a sixfold increase in installed capacity during the forecast period [7].

It has been investigated that battery energy storage systems (BESSs) have the ability to realize the renewable generation accommodation [8], perform peak shaving and valley filling [9], provide frequency regulation service [10], which help to improve the reliability of the power system. In order to meet the application requirements, a large number of battery cells are connected in series or parallel in a BESS, and the output characteristics of the energy storage system directly determine its performance. This structure enables the battery storage to meet the needs of utility companies with large-scale storage requirements, while at the same time, the aging and failures of internal batteries would cause the performance of the battery storage to degrade. In the process, the contribution of the BESS to improving the reliability of the power system is reduced, making it necessary to analyze the reliability of the BESS, so as to assess its impact on the power system reliability.

So far, reliability assessment techniques for BESSs have been extensively studied. It has been concluded that the benefits of energy storage in improving power system reliability depend on different factors such as charging/discharging power, energy capacity, and initial energy level of these units [11]-[12]. Meanwhile, since the BESS is an energy-limited and time-dependent resource whose ability to serve the power system depends on its prior operation, it is difficult to estimate its impact on power system reliability [13]. Related papers mainly characterize the BESS as a system with available and unavailable states, or further consider its diverse values of the state of charge (SOC), where the performance level of the BESS was mostly ignored [14]-[15], and there have been few studies on the detailed modeling of the BESS considering its internal topology. Besides, most of the existing studies do not regard the performance degradation of batteries under thermal conditions as a key factor to decrease the reliability of BESSs. An economic-degradation model has been proposed in [16] to demonstrate the effect of operational strategies on the lifespan of the energy storage plants. However, the battery degradation mentioned refers to the aging of the entire BESS, and the degradation of batteries inside has not been modeled separately. Reference [17] has introduced a method to evaluate the reliability of the battery module considering the state of health of the battery cell, but the model has not quantified the performance of the BESS, such as its energy storage and power output capability.

Moreover, thermal safety for the BESS has been increasingly concerned all around the world because of the occurrence of thermal runaway (TR) incidents nowadays [18]. TR is a potentially fatal phenomenon in which the battery involved enters an uncontrollable, self-heating state. In a BESS consisting of a great many cells, after a first runaway, the heat released is transferred to the surroundings, which may lead to the triggering of TRs in adjacent cells, and may also cause secondary disasters such as combustion and explosion. This so-called TR propagation is a major hazard to the safe and reliable operation of the BESS. In reference [19], it is estimated that the heat released by all batteries in an electric vehicle can be equivalent to a sudden energy output of 198.6 kg TNT when the TR is fully propagated. The cause of the Beijing lithium battery explosion on April 16, 2021, which killed two firefighters, is also believed to be the continuous TR in the BESS [20].

There have been significant research efforts on thermal reaction theories, TR mechanism, and power system reliability with dynamic-security considerations. Some models have been established to characterize chemical reactions in TR [21]-[22], TR propagation in a large-format battery module has been simulated to analyze the influence of module configuration

[23], and mitigation techniques have been proposed to help overcome the safety concerns of TR [24]. From a reliability point of view, cascading effects associated with large disturbances may lead to system inadequacy or instability, so it is valuable to capture the dynamic aspects of BESS behavior in TR propagation [25]-[26]. However, relevant studies have not considered the impact of TR propagation on the reliability of large-scale BESS, including the degradation of battery performance caused by the increase in temperature during TR propagation, and the sudden performance drop of the system due to successive failure of batteries.

The negligence of thermally-induced incidents leads to a lower-than-expected performance of the BESS. In the case that battery energy storage plays an important role in the renewable power system, it may cause severe curtailment of renewable energy or load, resulting in grid frequency collapse, power outages and economic losses.

To bridge these research gaps, the performance degradation of battery cells at different ambient temperatures, SOC values and the structure of the battery module are discussed, so that a multi-state reliability model of the BESS is established to describe its performance levels and corresponding probabilities. A TR propagation model is constructed based on relevant theories to predict the temporal sequence of batteries reaching the critical temperature of TR, and an assessment framework for investigating the reliability of large-scale BESS integrated power systems is proposed. The main contributions of this paper can be summarized as:

- Considering the thermally-induced degradation and complete failure, a multi-state reliability model that quantifies the performance of the BESS by its energy storage and power output capability is proposed. In this model, the degradation behavior of each internal cell is described, the universal generating function (UGF) method is adopted for aggregating all the batteries to obtain the real-time performance of the BESS. Moreover, the developed model incorporates the combined effects of sequential TR and the performance degradation of the surrounding batteries due to heat absorption.
- A reliability assessment framework of renewable power systems considering thermal-induced incidents of BESSs is established. Based on the Monte Carlo method, scenarios that reflect the uncertainties of the intermittent wind generation and fluctuating loads are simulated, and an optimal scheduling model is used to calculate the dispatched power of the BESS within its time-varying performance range. The reliability indices comprise the expected energy not supplied, the loss of load probability and the wind energy curtailment, realizing generation-demand coordination in reliability assessment.
- To efficiently solve the temporally coupled optimal scheduling model, a solution algorithm is proposed. In failure scenarios where no TR incidents occur, some linearization and approximation techniques are applied to ensure the feasibility of the solution. A performance update loop is presented in the solution process to invoke the multi-state model if there is TR propagation.

The remainder of the paper is organized as follows. Section II analyzes the reliability of BESS integrated renewable power systems. The multi-state model of the BESS considering real-time temperature is established in Section III. Section IV introduces the developed framework for reliability assessment of renewable power systems. Case studies are given in Section V, followed by the conclusions drawn in Section VI.

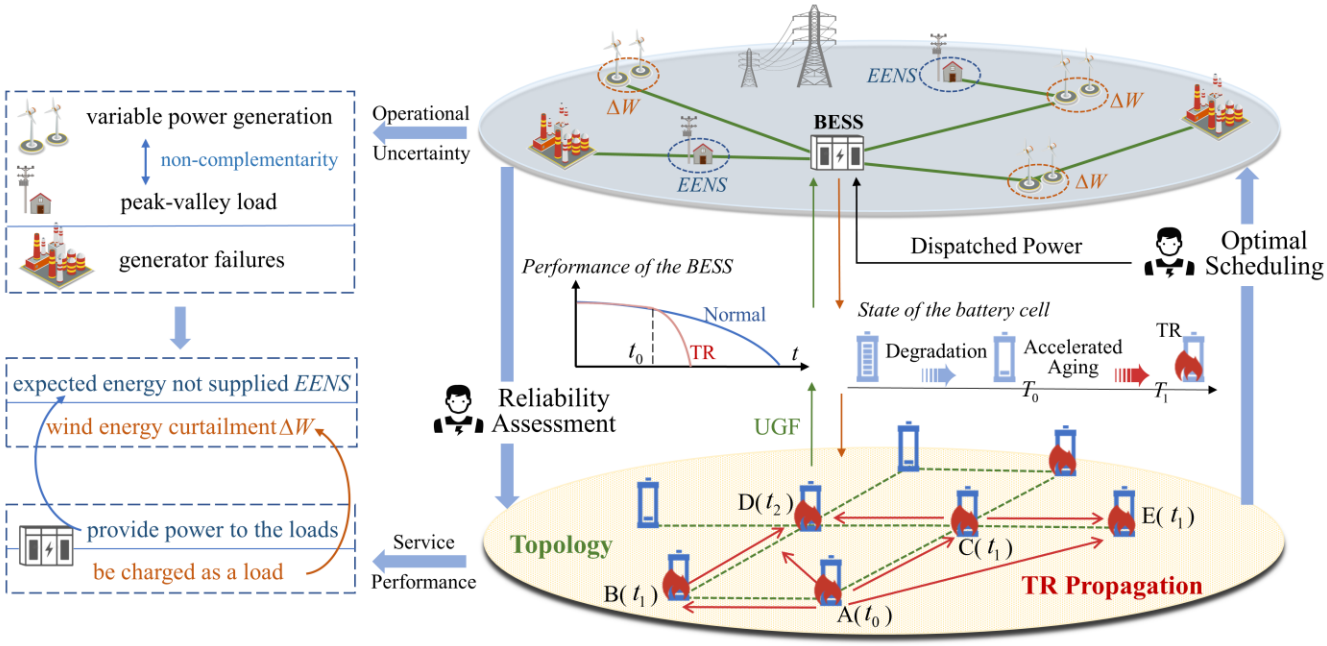

Fig. 1. Reliability analysis of BESS integrated renewable power systems.

II. Reliability Analysis of BESS Integrated Renewable Power Systems

Fig. 1 presents a general overview of the reliability analysis of BESS integrated renewable power systems conducted in this paper. The intermittency of wind power creates operational uncertainty for renewable power systems. For example, high-yield wind power at night does not coincide with peak loads, leading to the load curtailment during peak demand periods and the wind energy curtailment when the wind energy is oversupplied. The system is at greater risk when conventional generating units fail occasionally. The BESS plays an important role in the power system with a high proportion of renewable energy. It can either provide power to the loads or be charged as a load, which is of great significance to maintaining the safe and stable operation of the power system. In power system scheduling, the dispatchable power of the BESS is restricted by its real-time performance, and the contribution of the BESS to the power system is often evaluated by reliability indices.

There are a large number of battery cells in the BESS whose states directly determine the performance level of the entire system. Throughout the whole lifetime, battery degradation continues, limiting its energy storage and power output capability. Since both idle time and operating time occupy a significant part of the BESS life, calendar degradation and cycle degradation of the battery should be considered [27]. Generally, a battery degrades with a decrease in capacity and increase in resistance, which leads to the battery capacity fade and power fade [28]. Therefore, although batteries are usually characterized as either normal operation or complete failure in conventional reliability analysis, during actual operation, batteries need to be described by multiple states representing various performance levels.

It is worth noting that temperature and SOC have a strong impact on the aging rate of batteries, and the influencing mechanism is complicated. As depicted by the capacity fade curves obtained from the calendar aging studies and accelerated life tests, battery aging speeds up at certain SOC ranges as well as at high temperatures [29]-[31].

In addition to gradual performance degradation, sudden failures such as internal short-circuit, battery leakage and TR can significantly impair the performance of the battery or cause complete failure. Such failures are prone to occur at abnormal temperatures. Among them, TR has a great influence on the reliability of the BESS due to the characteristic of being able to propagate among batteries. As shown in Fig. 1, the heat absorption causes the temperature of battery A to increase from T_0, and the overheating condition results in its accelerated aging. After reaching the critical temperature T_1 of TR at time t_0, battery A completely fails, releases heat, and the TR further spreads, which degrades the performance of the BESS quickly.

To sum up, battery degradation and TR propagation are crucial factors affecting the performance of BESSs, which cannot be ignored in the reliability assessment of BESS integrated renewable power systems.

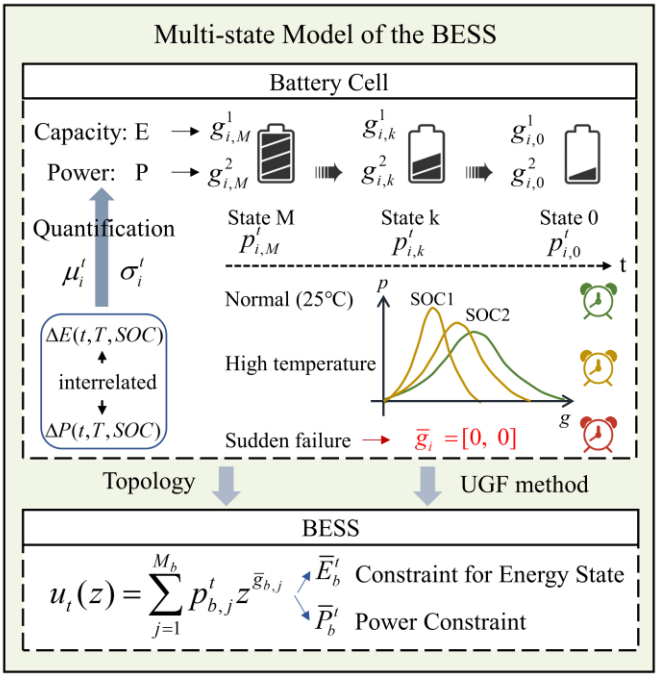

Fig. 2. Framework for multi-state model of the BESS.

III. Multi-State Model of the BESS Considering Real-Time Temperature

Based on the characteristic it exhibits during operation, detailed modeling of battery cell is conducted, as shown in Fig. 2. In this paper, battery aging is quantified by battery capacity loss and associated power changes. Specifically, according to the study of battery aging mechanisms, the calculation methods of calendar aging rate and cycle aging rate considering temperature and SOC are derived. Formulas for capacity loss are rewritten in the discrete form to adapt to different working conditions of the battery. Moreover, the relationship between the maximum output power and the resistance increase is summarized to quantify the power fade during battery degradation. In the proposed multi-state model, the state description of the battery cell can be obtained by using its performance distribution law. The UGF method is used for aggregating all the batteries to obtain the multi-state model of the BESS.

A. Reliability Description of the Battery Cell

1) Multiple states of the battery

To achieve a more accurate representation of the battery cell, a multi-state model is established [32], where the capacity of the battery is regarded as the performance measure.

It is assumed that battery cell i for $1 \le i \le n$ has M_i different states, thus the capacity of cell i is divided into M_i levels, corresponding to each performance state that occurs sequentially during battery degradation. All the battery performance levels are represented by the set G_i.

$$G_i = \left\{ g_{i,0}^1, g_{i,1}^1, \ldots, g_{i,M_i}^1 \right\} \tag{1}$$

where $g_{i,j}^1$ is an assigned value representing a range of capacity

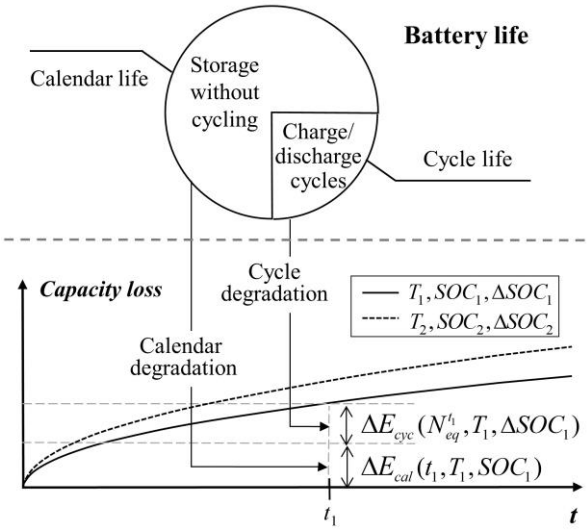

Fig. 3. Battery degradation and its quantification.

values $[g_{i,j}^{1\_lower}, g_{i,j}^{1\_up}]$.

Meanwhile, the state probabilities are grouped in the set $Y_i^t = \left\{ p_{i,0}^t, p_{i,1}^t, \ldots, p_{i,M_i}^t \right\}$, where $p_{i,j}^t$ is interpreted as the probability of cell i falling into state j at time t.

During battery degradation, the capacities of different cells are usually assumed to follow a normal distribution $N(\mu, \sigma^2)$ at any instant of time except the very beginning [17], and the mean value μ of the capacity distribution can be obtained from the battery capacity loss.

2) Calculation of capacity fade

As illustrated in Fig. 3, battery degradation can be divided into calendar degradation and cycle degradation. The former refers to the aging when the battery is stored without cycling, and the latter occurs during charge and discharge cycles [28]. The rates of both calendar degradation and cycle degradation are affected by temperature and SOC.

a) Calendar Degradation: Throughout the whole battery life, the capacity loss due to calendar degradation ΔE_{cal} can be expressed by (2) in the form of the Eyring law [30]. This equation implies that the capacity fade for every battery cell follows the same shape $f(t)$, the magnitude of which varies with a factor dependent on temperature T and SOC.

$$\Delta E_{cal}(t, T, SOC) = A_{SOC} \cdot \exp\left(-\frac{E_{a,SOC}^{cal}}{k_B T} \right) \cdot f(t) \tag{2}$$

where k_B is the Boltzmann constant. Pre-exponential factor A_{SOC} and activation energy $E_{a,SOC}^{cal}$ change in terms of SOC.

The chosen $f(t)$ can be a power of time t^z with a fixed z, assigned as $z = 1$ in [30], which means that the calendar aging rate is assumed to be a constant under the reference condition. In this paper, the battery capacity loss caused by calendar degradation over time period $\Delta\tau$ is calculated by multiplying the aging rate by time, considering the effects of temperature T^τ and battery SOC^τ at idle. Since the battery may be in a changing condition, ΔE_{cal} for battery i up to time t can be obtained using equation (3).

$$\Delta E_{cal,i}^t = \sum_{\tau=1}^{t-1} A_{SOC_i^\tau} \cdot \exp\left(-\frac{E_{a,SOC_i^\tau}^{cal}}{k_B T_i^\tau} \right) \cdot \Delta\tau \tag{3}$$

b) Cycle Degradation: As shown in (4), a power-law equation is used to describe the relationship between battery capacity loss ΔE_{cyc} and equivalent full cycles N_{eq}, thereby quantifying the cycle degradation at the reference temperature T_{ref} and over the reference SOC range [31]. In this equation, the values of $B_{\Delta SOC}$ and $C_{\Delta SOC}$ are related to SOC range ΔSOC during cycling and a temperature influence factor k_T is included.

$$\Delta E_{cyc}(N_{eq}, T, \Delta SOC) = B_{\Delta SOC} \cdot (N_{eq}/100)^{C_{\Delta SOC}} \cdot k_T \tag{4}$$

$$N_{eq} = \frac{W_{tot}}{2 \cdot U^{nom} \cdot E^{ini}} \tag{5}$$

where is W_{tot} the accumulated energy throughput of the cycled cell, U^{nom} is the nominal battery voltage and E^{ini} is the initial battery capacity.

The Arrhenius equation which gives the dependence of the rate constant of a chemical reaction on temperature has a vast application in developing battery lifetime models. Based on the form of the Arrhenius equation and a large number of experimental results, the influence of temperature on the battery capacity loss can be expressed as equation (6).

$$k_T = \exp\left(\frac{-E_a^{cyc}}{k_B} \left(\frac{1}{T} - \frac{1}{T_{ref}} \right) \right) \tag{6}$$

where E_a^{cyc} is the activation barrier for battery cycle aging.

Considering that battery i may charge/discharge under different operating conditions, its capacity loss due to cycle degradation $\Delta E_{cyc,i}^t$ to time t can be rewritten as follows.

$$\Delta E_{cyc,i}^t = \sum_{\tau=1}^{t-1} \frac{Bc \cdot k_{T_i^\tau}}{200 U_{norm} E^{init}} (N_{eq,i}^{\tau-1}/100)^{c-1} P_i^\tau \Delta\tau \tag{7}$$

where P_i^τ is the charging/discharging power of i at time τ.

On this basis, the mean value μ_i^t of the capacity distribution corresponding to battery cell i at time t can be obtained by subtracting the total capacity fade from its initial capacity, and the standard deviation σ_i^t is as follows [33].

$$\mu_i^t = E_i^{init} (1 - \Delta E_{cal,i}^t - \Delta E_{cyc,i}^t) \tag{8}$$

$$\sigma_i^t = \frac{1 - \mu_i^t / E_i^{ini}}{6} \tag{9}$$

Therefore, each probability in the set Y_i^t can be calculated.

$$p_{i,j}^t = F(g_{i,j}^{1\_up}) - F(g_{i,j}^{1\_lower}) \tag{10}$$

where F is the cumulative distribution function of the normal distribution $N(\mu_i^t, \sigma_i^{t2})$.

3) Quantification of power fade

In addition to the energy storage capability represented by

$g_{i,j}^1(0 \le j \le M_i)$, $g_{i,j}^2(0 \le j \le M_i)$ is introduced to reflect the power output capability of battery cell i in different states.

According to the impedance model of battery, as the cell ages, its polarization resistance does not change significantly, whereas the ohmic resistance increases, causing the battery power to fade. The state of health (SOH) can be used to quantify the degradation severity of the battery cell, and the relationship between ohmic resistance and SOH has been found [34]:

$$SOH_i^t = \frac{E_i^t - E_i^{end}}{E_i^{init} - E_i^{end}} \tag{11}$$

$$R_i^t = R_i^{ini}\left(1 + k_r(1 - SOH_i^t)\right) \tag{12}$$

where E_i^t is the residual capacity of cell i at time t, E^{end} is the capacity at the end of the battery life, R_i^t is the ohmic resistance of cell i at time t, R_i^{ini} represents the initial ohmic resistance of cell i, and k_r is the regression coefficient for the linear relationship between ohmic resistance and SOH.

During battery charging, the maximum power can be reached when the voltage reaches its maximum value [35]. Then, the maximum power of the battery cell is supposed to be inversely proportional to its internal resistance. Combining the equations above, the power output capability $g_{i,j}^2$ of cell i in state j can be derived.

$$g_{i,j}^2 = \frac{P_i^{ini}}{1 + k_r\left(1 - \dfrac{g_{i,j}^1 - E_i^{end}}{E_i^{init} - E_i^{end}}\right)} \tag{13}$$

Therefore, the corresponding UGF used to represent the multi-state model of battery cell i at time t is defined as [36]:

$$u_{i,t}(z) = \sum_{j=1}^{M_i} p_{i,j}^t \cdot z^{(g_{i,j}^1, g_{i,j}^2)} \tag{14}$$

B. Thermal Runaway Propagation Procedure of the BESS

Once a battery cell in the BESS experiences TR and releases heat, the heat is absorbed by surrounding batteries with different transfer efficiencies. Temperatures of corresponding batteries increase, accelerating the rates of side reactions, causing the batteries to decay faster, and further triggering a series of TR when a certain temperature is reached. Fig. 4 illustrates the process of TR propagation in the BESS.

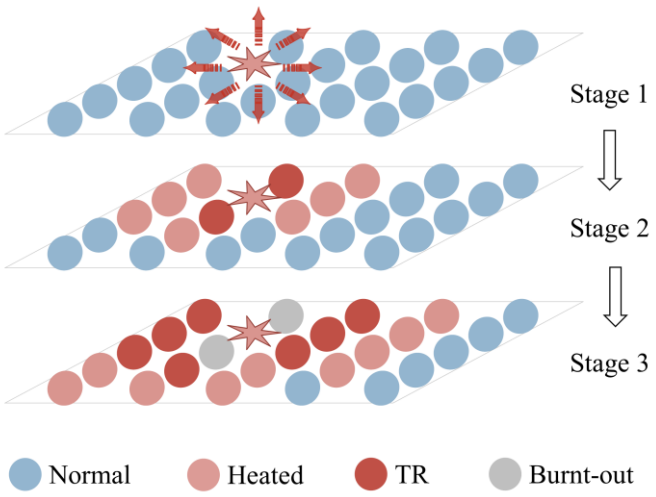

Fig. 4. The process of TR propagation in the BESS.

TABLE I
FACTORS INFLUENCING TR PROPAGATION

Factor	Specific Impact	Ref
cell-to-cell spacing	Determines the spatial extent in which heat transfer occurs. In the process of TR propagation, the contribution of thermal convection is not significant, the main forms of heat transfer are thermal conduction and thermal radiation, and the heat transfer efficiency between battery cells decreases with the increase of their spacing.	[37]
SOC	Affects the severity of TR. When TR is triggered, the energy released by the battery is related to its SOC. It has been proved that the heat released by lithium iron phosphate battery during TR is in a range, and its value is positively correlated with the SOC.	[38]
battery pack topology	Determines the different distances between cells, resulting in differences in heat transfer efficiency. In addition, the battery in the parallel branch acts as a short-circuit load after TR happens, and normal batteries of the external circuit input electrical energy to it to generate Joule heat, which accelerates heat release and increases the maximum temperature of TR.	[39]

1) Factors Influencing TR Propagation

Regarding the influencing factors of TR propagation, relevant research has been carried out, and there is evidence that factors such as cell-to-cell spacing, SOC and battery pack topology affect the heat transfer between batteries. The factors considered in this paper are shown in Table I.

2) TR Propagation Analytics Based on Battery Thermal Dynamics

During TR propagation, heat transfer occurs between any two battery cells within the effective range. To describe the process, the exothermic and endothermic behavior of each cell in the BESS needs to be modeled.

First, battery cell i on performance level j triggers initial TR with probability $p_{i,j}^{TR}$, which varies with time. After that, the potential risk of TR is transmitted within the BESS, and the heat energy $H_{i,r}^t$ absorbed by the nearby cell r from cell i is written as follows.

$$H_{i,r}^t = \sum_{\tau=1}^{t-t_{i0}} P_i^{REL,\tau} \cdot \eta_{i,r} \cdot \Delta\tau \tag{15}$$

where $P_i^{REL,\tau}$ represents the heat release rate of battery cell i at time τ, $\eta_{i,r}$ represents its efficiency in transferring heat to r, and t_{i0} is the moment at which battery i triggers TR.

Considering various influencing factors comprehensively, the heat release rate of battery i and the heat transfer efficiency between batteries can be determined based on Table I.

$$P_i^{REL,t} = P^{REL,t} \cdot SOC_i^{t_{i0}} \cdot n_i^{t_{i0}} / k_i^{REL} \tag{16}$$

$$\eta_{i,r} = \begin{cases} \eta_{thc}/d_{i,r} + \eta_{thr}/{d_{i,r}}^3, & d_{i,r} \le d_0 \\ 0, & d_{i,r} > d_0 \end{cases} \tag{17}$$

where $P^{REL,t}$ is the heat release rate at time t corresponding to

the typical TR heat release rate curve of this type of lithium-ion battery, $SOC_i^{t_{i0}}$ represents the SOC of battery i when TR is triggered. At this time, the current from $n_i^{t_{i0}}$ normal parallel branches in the BESS flows through the failed battery cell i, k_i^{REL} is a constant, $d_{i,r}$ is the distance between battery i and battery r, η_{thc} and η_{thr} are constants, respectively, as the reference efficiencies of heat conduction and heat radiation in the given environment.

With the absorption of heat, the temperature of the battery gradually increases, and the criterion for the battery to trigger TR is that its temperature reaches the critical temperature T_{crit} of TR.

$$T_r^t = T_t^{t_{i0}} + \sum_i \frac{H_{i,r}^t}{c_r m_r}, \quad i \in \{u_i^t = 1\} \tag{18}$$

$$u_r^t = \begin{cases} \max\left(u_r^{t-1}, 0\right), & T_r^t < T_{crit} \\ 1, & T_r^t \geq T_{crit} \end{cases} \tag{19}$$

where T_r^t represents the temperature of battery r at time t, u_r^t is used to indicate whether TR occurs in battery r at time t, with a value of 1 indicating that TR is triggered at this time and 0 representing no TR. c_r and m_r are specific heat capacity and mass of battery r, respectively.

C. Multi-State Model of the BESS

In the process of TR propagation, batteries that are triggered into TR enter the state of complete failure, and temperatures of surrounding batteries rise, resulting in an abnormal operating condition of overheating, which may trigger a series of failures while accelerating degradation. Therefore, the distribution of battery capacity at this time is different from that under normal conditions.

For a BESS with N batteries, $T_t = [T_1^t, T_2^t, \ldots, T_N^t]$ contains the temperatures of all battery cells at time t. The mean value $\mu_i^t (1 \leq i \leq N)$ and standard deviation $\sigma_i^t (1 \leq i \leq N)$ of the capacity distribution corresponding to each battery at this time can be calculated according to equations (8) and (9), respectively.

On this basis, the probabilities that each battery cell falls in different performance states are calculated, and the performance probability vector P_t of the batteries is obtained.

$$P_t = [Y_1^t, \ldots, Y_N^t] = [p_{1,0}^t, \ldots, p_{1,M_1}^t, \ldots, p_{N,0}^t, \ldots, p_{N,M_N}^t] \tag{20}$$

The performance level and state probability of the BESS are based on the characteristics of constitutive battery cells. For a parallel structure, the overall performance level is equal to the sum of the performance levels of all components. For a series structure, the total maximum power is equal to the sum of the maximum power of all the cells in it, and the total residual capacity is determined by the worst cell. Using the UGF method, the composition operator Φ considering the topology of the battery pack is defined, and the performance states and corresponding probabilities of battery cells are mapped to the performance distribution of the BESS. In this way, the multi-state model of the BESS is established.

$$\begin{aligned} u_{b,t}(z) &= \Omega_\phi\left(u_{1,t}(z), u_{2,t}(z), \ldots, u_{N,t}(z)\right) \\ &= \sum_{j_1=0}^{M_1} \sum_{j_N=0}^{M_N} p_{1,j_1}^t \cdots p_{N,j_N}^t z^{\Phi\left((g_{1,j_1}^1, g_{1,j_1}^2), \ldots, (g_{N,j_N}^1, g_{N,j_N}^2)\right)} \\ &= \sum_{j=1}^{M_b} p_{b,j}^t z^{(g_{b,j}^1, g_{b,j}^2)} \end{aligned} \tag{21}$$

$$\Phi(g_{1,j_1}^1, \ldots, g_{N,j_N}^1) = \begin{cases} \sum_{i=1}^{N} g_{i,j_i}^1, & \textit{cells in parallel} \\ \min(g_{1,j_1}^1, \ldots, g_{N,j_N}^1), & \textit{cells in series} \end{cases} \tag{22}$$

$$\Phi(g_{1,j_1}^2, \ldots, g_{N,j_N}^2) = \sum_{i=1}^{N} g_{i,j_i}^2 \tag{23}$$

where $\bar{g}_{b,j} = (g_{b,j}^1, g_{b,j}^2)$ and $p_{b,j}^t$ are the performance states and corresponding probabilities of the BESS, respectively, and M_b is its number of performance states.

Therefore, the residual capacity and maximum power of the BESS b at time t are denoted as $\bar{E}_b^t$ and $\bar{P}_b^t$, respectively.

$$\bar{E}_b^t = \sum_{j=1}^{M_b} p_{b,j}^t g_{b,j}^1 \tag{24}$$

$$\bar{P}_b^t = \sum_{j=1}^{M_b} p_{b,j}^t g_{b,j}^2 \tag{25}$$

An example of using the multi-state model to represent a BESS is given in Fig. 5. To obtain the performance of the BESS at time t_1+1, the degradation of internal battery cells should be analyzed first. Based on the temperature, SOC value and operating data of each battery in each period, the capacity loss up to time t_1+1 can be calculated separately using equations (3) -(7). It is worth noting that the proposed TR propagation model is used to get the real-time temperature of the battery cell in case of a TR incident. The mean value $\mu_i^{t_1+1}$ and standard deviation

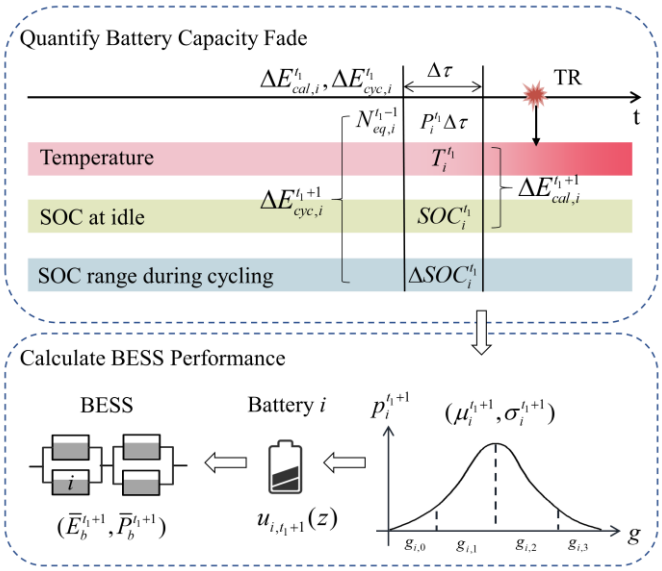

Fig. 5. Example of using the multi-state model.

$\sigma_i^{t_1+1}$ of the capacity distribution for each cell can then be obtained to calculate the probabilities that they are in different states. When the UGFs of battery cells are generated, the time-dependent performance of the BESS can be determined by the use of the UGF method considering the topological structure of the battery module.

IV. Reliability Assessment Framework of BESS Integrated Renewable Power Systems

In order to investigate the reliability of renewable power systems considering thermally-induced incidents of large-scale battery energy storage, an assessment framework is created. On the basis of constructing models to describe conventional generating units, wind turbines and the BESS, this paper proposes a Monte Carlo simulation-based algorithm, in which an optimal scheduling model is deployed. In each simulated power system operating scenario, the wind power output and the failure of each unit are randomly generated based on statistical data. The dispatched power of generating units and the charging/discharging power of the BESS are optimally scheduled in each period, thereby the proposed reliability indices can be calculated.

A. Optimal Scheduling of the BESS

Failures of generating units and the BESS, and the uncertainty characteristics of wind power lead to a decrease in the operational reliability of the power system. To illustrate the impact of BESS performance on the system reliability, an optimal scheduling model considering battery performance degradation and TR propagation in BESS is built.

In this paper, each generating unit is modeled as a two-state component that enters a failure state with a certain probability, the BESS is depicted with the multi-state reliability model, and the wind generation model is referred to [40]. The objective of the scheduling model is to minimize the total system cost over the studied horizon, as denoted in (26). In the objective function, the first two terms $C_g(P_g^t)$ and $C_w(P_w^t)$ represent the generation costs of conventional units and wind turbines, respectively. $C_b\left(\left|P_b^t\right|\right)$ is the operation cost of BESS, in which $\left|P_b^t\right|=\left|P_{ch}^t-P_{dis}^t\right|$ is the absolute value of the charge/discharge power. $C_{m,l}(PC_m^t)$ denotes the compensation cost of load curtailment and $C_p(\Delta P_w^t)$ is the penalty for wind curtailment.

$$Min\ f=\sum_{t=1}^{N_T}\sum_{m=1}^{N_M}\left[\begin{array}{l}\sum_{g=1}^{NG_m}C_g(P_g^t)+\sum_{w=1}^{NW_m}C_w(P_w^t)+\sum_{b=1}^{NB_m}C_b\left(\left|P_b^t\right|\right)\\+C_{m,l}(PC_m^t)+\sum_{w=1}^{NW_m}C_p(\Delta P_w^t)\end{array}\right] \tag{26}$$

where N_T is the number of time steps in the studied period, N_M is the number of nodes, NG_m, NW_m and NB_m are numbers of conventional generating units, wind turbines and BESSs at node m respectively.

The objective function is subject to the following constraints.

Generating unit constraints:

$$P_g^{\min}\le P_g^t\le P_g^{\max},\ \ 0\le P_w^t\le P_w^{t,avl} \tag{27}$$

$$Q_g^{\min}\le Q_g^t\le Q_g^{\max},\ \ Q_w^{\min}\le Q_w^t\le Q_w^{\max} \tag{28}$$

$$P_g^t+RD_g\le P_g^{t+1}\le P_g^t+RU_g \tag{29}$$

Equations (27) and (28) restrict the power output bounds of conventional generating units and wind turbines. The ramp-up and ramp-down constraints are presented in (29).

BESS constraints:

$$0\le x_{b,ch}^t+x_{b,dis}^t\le 1 \tag{30}$$

$$0\le P_{b,ch}^t\le x_{b,ch}^t\bar{P}_b^t,\ \ 0\le P_{b,dis}^t\le x_{b,dis}^t\bar{P}_b^t \tag{31}$$

$$SOC_b^{t+1}\cdot\bar{E}_b^{t+1}=SOC_b^t\cdot\bar{E}_b^t+\eta_b P_{b,ch}^t\Delta t-\frac{P_{b,dis}^t\Delta t}{\eta_b} \tag{32}$$

$$SOC_b^{\min}\le SOC_b^t\le SOC_b^{\max} \tag{33}$$

$$SOC_b^0=SOC_b^{N_T} \tag{34}$$

where $x_{b,ch}^t$ and $x_{b,dis}^t$ are binary variables, $x_{b,ch}^t=1$ and $x_{b,dis}^t=1$ indicate that BESS b is in charging and discharging states at time t, respectively. $P_{b,ch}^t$ and $P_{b,dis}^t$ represent the optimized charging and discharging power of the BESS at time t, respectively. η_b is the charging/discharging efficiency of the BESS, SOC_b^t is the SOC of BESS b at time t, $SOC_b^{\min}$ and $SOC_b^{\max}$ are the minimum and maximum SOC of the BESS in the set range. SOC_b^0 and $SOC_b^{N_T}$ in (34) denote the SOC value at the beginning and end of the scheduling period, respectively.

Load curtailment constraints:

$$0\le PC_m^t\le PD_m^t \tag{35}$$

Power system operation constraints:

$$\begin{aligned}&\sum_{g,w,b\in\Psi_{C,m}}(P_g^t+P_w^t+P_b^t)-(PD_m^t-PC_m^t)\\&=\sum_{s\in\Psi_{N,m}}V_m^tV_s^t\left[G_{ms}\cos(\theta_m^t-\theta_s^t)+B_{ms}\sin(\theta_m^t-\theta_s^t)\right]\end{aligned} \tag{36}$$

$$\begin{aligned}&\sum_{g,w,b\in\Psi_{C,m}}(Q_g^t+Q_w^t+Q_b^t)-QD_m^t\\&=\sum_{s\in\Psi_{N,m}}V_m^tV_s^t\left[G_{ms}\sin(\theta_m^t-\theta_s^t)+B_{ms}\cos(\theta_m^t-\theta_s^t)\right]\end{aligned} \tag{37}$$

$$V_m^{\min}\le V_m^t\le V_m^{\max} \tag{38}$$

$$\theta_m^{\min}\le\theta_m^t\le\theta_m^{\max} \tag{39}$$

$$\left|S_{ms}^t\right|=\left|P_{ms}^t+jQ_{ms}^t\right|\le S_{ms}^{\max} \tag{40}$$

Equations (36) and (37) denote the power balance constraints considering active and reactive power. Equations (38) and (39) specify the nodal voltage and angle bounds, respectively. In equation (40), a capacity limit is imposed on each transmission line.

B. Reliability Indices

Generally, the reliability of a multi-state system is defined as the probability that the performance level of the system is higher than the required [42]. Assuming that the minimum

performance requirement of the BESS is γ, its reliability Rel_b^t at time t can be obtained from (41) after the performance states and corresponding probabilities of the system are calculated.

$$Rel_b^t = \sum_{\bar{g}_{b,j} \geq \gamma} p_{b,j}^t \tag{41}$$

To evaluate the risk of power system, the expected energy not supplied ($EENS_m$) and the loss of load probability ($LOLP_m$) are introduced [43], and the wind energy curtailment (ΔW_t) is also proposed in this paper to reveal the renewable energy accommodation capability of the system.

After calculating the load curtailment PC_m^t of node m and the wind curtailment ΔP_w^t of wind turbine w at time t, the reliability indices $EENS_m$, $LOLP_m$ and ΔW_t can be calculated as:

$$EENS_m = \sum_{st=1}^{ST} \sum_{t=1}^{N_T} PC_m^t \Big/ ST \tag{42}$$

$$LOLP_m = \sum_{st=1}^{ST} 1\left(\sum_{t=1}^{N_T} PC_m^t > 0 \right) \Big/ ST \tag{43}$$

$$\Delta W_t = \sum_{st=1}^{ST} \sum_{m=1}^{N_M} \sum_{w=1}^{NW_m} \Delta P_w^t \Big/ ST \tag{44}$$

C. Procedure Stages and Solution Methodology

The reliability assessment procedure for renewable power systems can be divided into three main steps. The first is to initialize the system parameters, the second is to simulate the operation of the power system within the studied period for a specified number of times using the Monte Carlo method. On this basis, the reliability indices are calculated in the third step. In order to efficiently solve the multi-state model of BESS within the time-coupled optimal scheduling model, a solution algorithm is proposed.

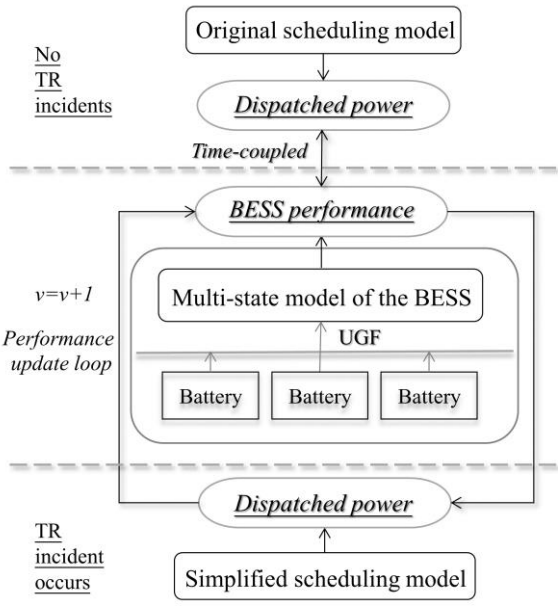

Fig. 6. Structure of the solution methodology.

As shown in Fig. 6, according to the performance change characteristics of the internal batteries, this paper divides the failure scenarios of the BESS into two categories based on whether the TR propagation occurs or not. If there is no TR incident during the scheduling period, it can be considered that the hourly capacity change rate of a single battery and the entire BESS is consistent. That is, after obtaining the initial value of BESS performance based on operating data and the multi-state model, the optimal scheduling model uses the time coupling relationship between the dispatched power and the overall performance of the BESS rather than the performance of each battery. Besides, some linearization and approximation techniques are applied to ensure the feasibility of the solution. The details are as follows.

At the beginning of the studied period, generate the UGF of each battery cell and calculate the residual capacity $\bar{E}_b^0$ and maximum power $\bar{P}_b^0$ of the BESS by equations (3)-(25). In the optimal scheduling model, equation (31) that enforce the BESS charging/discharging power constraints can be linearized by the big-M method as (45) [44].

$$\begin{aligned} 0 \leq P_{b,ch}^t \leq x_{b,ch}^t M, \quad P_{b,ch}^t \leq \bar{P}_b^t \\ 0 \leq P_{b,dis}^t \leq x_{b,dis}^t M, \quad P_{b,dis}^t \leq \bar{P}_b^t \end{aligned} \tag{45}$$

where M is a large constant.

Referring to the battery degradation equations derived in Section III, the hourly residual capacity of BESS can be obtained by (46), and the calculation of $\bar{P}_b^t$ can be linearly approximated by Taylor expansion.

$$\bar{E}_b^t = \bar{E}_b^0 (1 - \Delta E_{cal,b}^t - \Delta E_{cyc,b}^t) \tag{46}$$

$$\bar{P}_b^t = \bar{P}_b^0 + (\bar{E}_b^t - \bar{E}_b^0) \cdot \left(\frac{\bar{P}_b^0 k_r}{\bar{E}_b^0} \left(1 + k_r \left(1 - \frac{\bar{E}_b^0 - E_i^{end}}{E_i^{init} - E_i^{end}} \right) \right)^{-2} \right) \tag{47}$$

The time-coupled optimal scheduling model defined by (26)-(30), (32)-(40) and (45)-(47) is denoted as the original scheduling model, and its solution is $\mathbf{P}^{t,1} = [P_g^t, P_w^t, P_b^t]$.

However, in the TR incident, the performance changes of internal batteries are inconsistent, making it impossible to update the state of the BESS as a whole. Then, a performance update loop is presented in the solution process.

The first-round input to the BESS multi-state model is the hourly dispatched power of the BESS obtained by solving the original scheduling model, assuming no TR incidents occur. The performance update loop represents the interaction between the multi-state model and the simplified scheduling model, the latter being distinguished from the original scheduling model in that the hourly performance of the BESS is preset by the multi-state model. The two problems are calculated iteratively until the convergence is achieved. The convergence criterion is based on the iterative variation in system scheduling, which can be expressed as (48).

$$\sum_{t=1}^{N_T} \sum_{m=1}^{N_M} \left(\sum_{g=1}^{NG_m} \left| P_g^{t,v} - P_g^{t,v-1} \right| + \sum_{w=1}^{NW_m} \left| P_w^{t,v} - P_w^{t,v-1} \right| + \sum_{b=1}^{NB_m} \left| P_b^{t,v} - P_b^{t,v-1} \right| \right) \leq \varepsilon \tag{48}$$

Algorithm 1: Solution of the Optimal Scheduling Model

Input: parameters of components in the power system

1: Generate $(\bar{E}_b^0, \bar{P}_b^0)$ using (3)-(25)

2: **for** *st* = 1 to *ST* **do**

1: Generate the wind power scenario and failure scenario

2: $v \leftarrow 1$, assuming there is no TR incidents, calculate the hourly schedule $\mathbf{P}^{t,v}$ using the original scheduling model

3: **if** TR incident occurs during the scheduling period **do**

while convergence criterion (48) is not satisfied **do**

1. Update the BESS performance $\mathbf{G}^{t,v} = (\bar{E}_b^t, \bar{P}_b^t)$ by $\mathbf{P}^{t,v}$

2. Update the hourly schedule $\mathbf{P}^{t,v+1}$ by $\mathbf{G}^{t,v}$ using the simplified scheduling model

3. $v \leftarrow v+1$

end while

end if

end for

3. Calculate the reliability indices by (41)-(44)

Output: reliability indices Rel_b^t, $EENS_m$, $LOLP_m$ and ΔW_t

where $P_g^{t,v}$, $P_w^{t,v}$ and $P_b^{t,v}$ are respectively the dispatched active power of generator g, wind turbine w and BESS b at time t in iteration v. ε is a small tolerance.

The detailed solution algorithm is listed in Algorithm 1, and the calculation is accomplished by MATLAB R2018b. Using linearization techniques, the optimal scheduling model is transformed into a linear programming (LP) problem that can be solved by the CPLEX solver.

V. Case Studies

Case studies are conducted to validate the reliability assessment method of renewable power systems considering thermally-induced incidents of large-scale BESS. Firstly, the energy storage and power output capability of the BESS is evaluated by the multi-state model. Then, the impact of battery degradation and TR propagation upon the reliability of the BESS integrated power system is verified by the reliability assessment framework. Simulations are performed at different ambient temperatures and SOC values to reveal the relationship between these two factors and the service performance of the BESS. Furthermore, computational performance for larger systems are presented to justify the practical utility of the conducted research on large-scale systems.

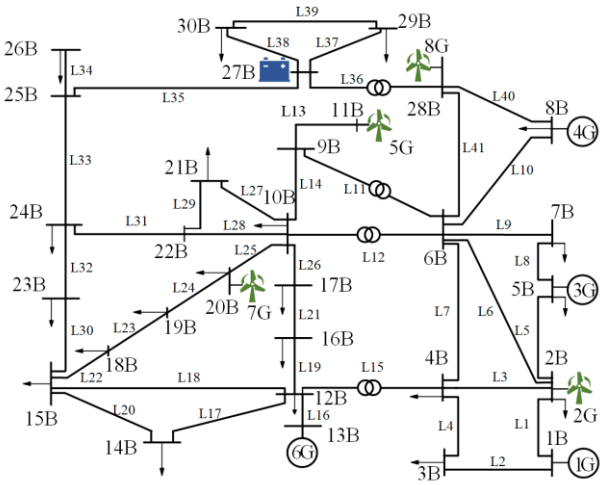

Fig. 7. Network topology of the modified 30-bus system.

TABLE II
PARAMETERS OF BATTERY CELL

	g_0	g_1	g_2	g_3	g_4	g_5
Performance (p.u)	[0.0, 0.1]	[0.1, 0.3]	[0.3, 0.5]	[0.5, 0.7]	[0.7, 0.9]	[0.9, 1.0]
Assigned value	0.0	0.2	0.4	0.6	0.8	1.0

The modified IEEE 30-bus system with 4 conventional generating units, 4 wind turbines and a BESS is reconstructed, as depicted in Fig. 7. The total generation capacity of wind turbines at nodes 2, 11, 20 and 28 is 75 MW, accounting for 41.28% of the installed capacity of the system. It is assumed that the BESS contains four identical battery modules in parallel. Each battery module consists of 50 parallel strings with 110 cells in series in each string, reaching a total capacity of 3.96 MWh. The maximum output power of the BESS is supposed to be 11.88MW. Each battery cell in the BESS is a high capacity lithium-ion battery and is modeled as a six-state component, whose parameters are given in Table II.

A. Energy Storage and Power Output Capability of the BESS

Each battery in the BESS is assumed brand-new at the beginning. Referring to the capacity fade curve fitted by the experimental results in [29]-[31], set the value of parameters in equations (3) and (7), so as to obtain the calculation formula of μ_i^t that conforms to the realistic degradation process of the battery. The simulation parameters are given in Table III.

Assuming that the number of charging/discharging cycles of the BESS is 1.5 times per day. The variations in residual capacity and maximum power (when $SOC_b = 100\%$) of the

TABLE III
BESS MODELING PARAMETERS

Parameters	Descriptions	Values	Units
U_i^{nom}	Nominal voltage of cell	6	V
E_i^{ini}	Initial capacity of cell	120	Ah
	Initial capacity of BESS	15.84	MWh
P_i^{ini}	Initial maximum power of cell	0.54	kW
	Initial maximum power of BESS	11.88	MW
T_{ref}	Reference temperature	25	°C
T_{amb}	Ambient temperature	25	°C
SOC	Battery SOC at idle	50	%
A	Coefficient of calendar aging	$3.115 \cdot 10^{11}$	/
E_a^{cal}	Activation energy for calendar aging	$4.557 \cdot 10^{-17}$	eV
ΔSOC	SOC range during cycling	20-80	%
E_a^{cyc}	Activation barrier for cycle aging	0.380	eV
B	Coefficient of cycle aging	3.708	/
C	Coefficient of cycle aging	0.452	/

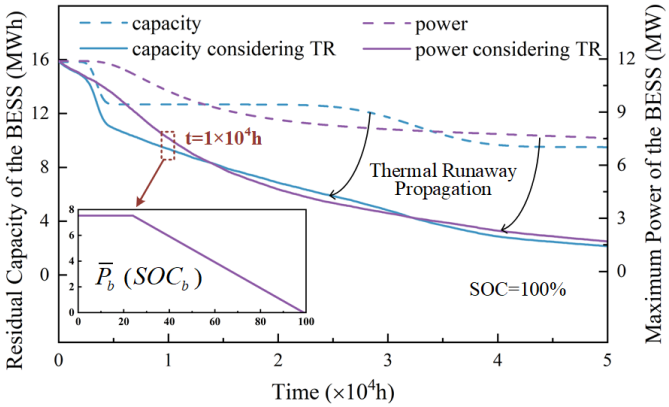

Fig. 8. Performance of the BESS in real time.

BESS versus time are plotted by the dotted lines in Fig. 8. From the figure, it can be seen that as the batteries decay during operation, the overall performance of the BESS also continuously declines, impairing its ability to provide services to the power system.

During the charging and discharging of a battery, abuse conditions and self-induction may lead to TR, and the rate of such an accident is assumed to be $\lambda = 5\times10^{-8}$ in this paper [45]. The product of the mass and specific heat capacity of the battery cell is supposed to be 1650 $\mathrm{J\cdot K^{-1}}$ and the critical temperature T_{crit} of TR is set to 260℃ [46]. The occurrence of TR causes the performance level of the corresponding battery to immediately drop to 0 and cannot be repaired. The heat release speed of TR refers to typical heat release curve of lithium ion battery in [47].

Considering TR propagation, the degradation of the BESS over time is quantified by simulating its operating scenarios, as shown by the solid lines in Fig. 8. Since the available power is dependent on the battery SOC, in addition to the results at $SOC_b = 100\%$, Fig. 8 also demonstrates the available charging power of the BESS at different SOC values at the SOH corresponding to $t = 1\times10^4 h$. It can be observed that, compared with the assessment results without the consideration for TR and its propagation, the system performance in all periods decreases. This is mainly because that the heat transfer between batteries during TR propagation causes the spread of failures, and the decay of a large number of cells results in the sudden decline in the system performance. Therefore, the reliability of the BESS is overestimated in conventional models, illustrating the necessity of considering TR propagation in the reliability assessment of the BESS.

To further show the impact of TR propagation on the reliability of the BESS, an accident scenario is randomly selected, and the reliability R_b^t of the BESS and the TR propagation path are given in Fig. 9. Assuming a performance threshold of $E_b^t \geq 0.8\times E_b^{ini}$ for the BESS, the reliability of the system decreases obviously with the aggravation of the TR incident. After the initial TR of battery v occurs at time $t = 0$, TR first propagates in the series branch due to the smaller spacing. The plot which shows the change in temperature of the

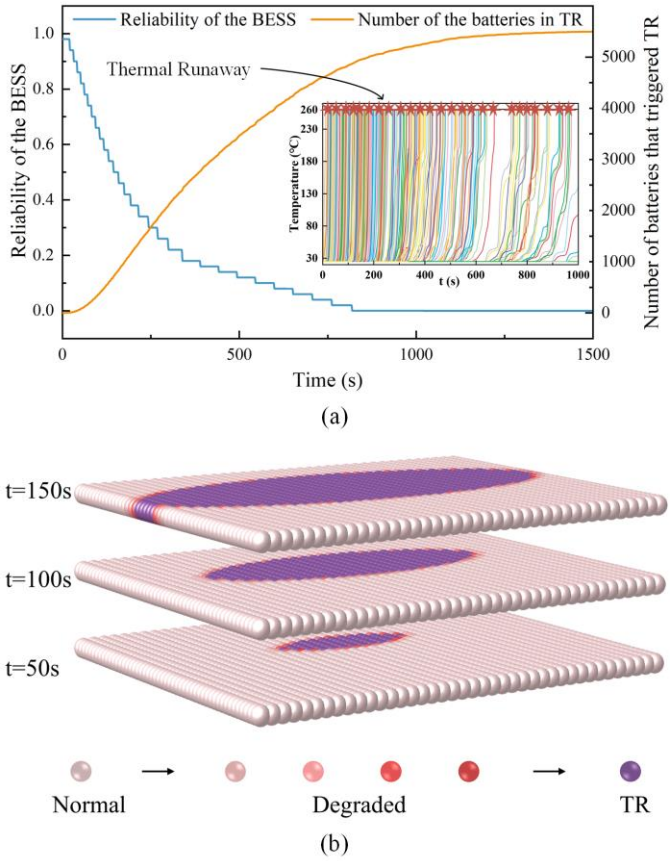

Fig. 9. An accident scenario. (a) Reliability of the BESS. (b) TR propagation path.

cells in the series and parallel branches adjacent to v proves it. When T_{crit} is reached in succession, the batteries trigger TR one by one, and the number of failed cells in the BESS gradually increases. After just 250 seconds, the reliability of the system drops to about 0.3. It is worth noting that the TR propagation path in Fig. 9 illustrates the spread of the accident near battery v. Besides, due to the relatively large space between battery modules, TR does not propagate to other modules in this scenario.

B. Comparison of System Reliability Assessed by Conventional and the Proposed Models

After a three-year operation of the BESS, simulation tests are implemented on the following three cases to assess the reliability of the power system. The entire studied period N_T is set as 24 hours.

Case 1: Regardless of the degradation during operation or special failures such as TR propagation, the BESS is simply modeled to operate in either perfect state or completely failure state. Considering the topology, the failure rate of the BESS is calculated using probability formulas according to the battery failure rate in [45].

Case 2: The impact of TR propagation is considered in this case regardless of the degradation during operation. In this case, the failure rate of the BESS set in case 1 is maintained, but the TR scenario is calculated separately. In the TR propagation path,

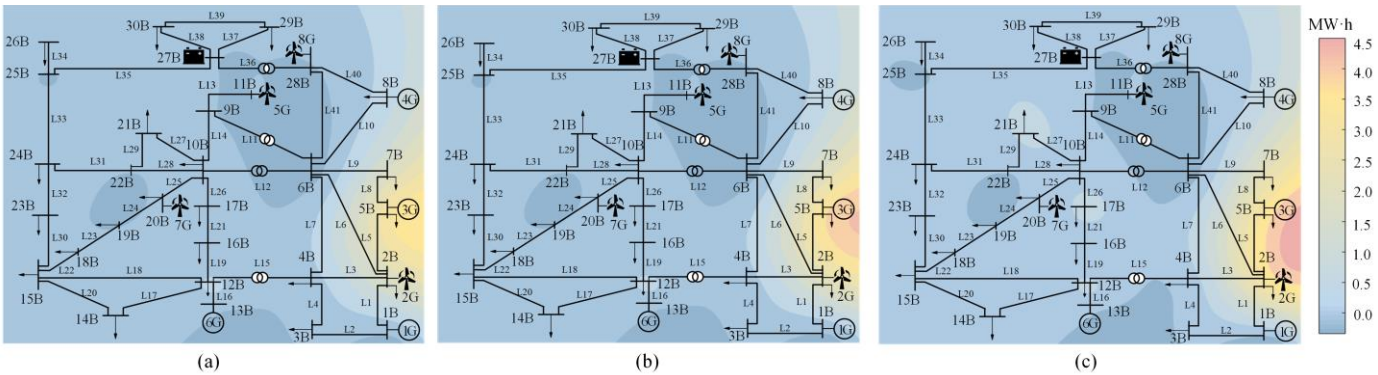

Fig. 10. Gradient distribution of the reliability indices $EENS_m$ for the three cases. (a) Case 1. (b) Case 2. (c) Case 3.

the battery reaching T_{crit} is regarded as failure, but the degradation of surrounding batteries at high temperature is not considered.

Case 3: The impacts of battery degradation and TR propagation on the reliability of the BESS are evaluated in this case. In this case, the BESS is modeled as a multi-state system, which differs from case 2 by considering the performance degradation of batteries during operation and TR incidents.

The gradient distributions of reliability indices $EENS_m (1 \le m \le 30)$ at different nodes for the three cases are shown in Fig. 10, where the background colors of subplots (a), (b) and (c) reflect the values of the corresponding indices. It is worth noting that only the values of the nodes are calculated in the simulation, and the colors of the remaining points are obtained by interpolation.

From a spatial perspective, transmission congestion leads to power outages in some regions with different probabilities. The deployment of the BESS can realize the electric energy time-shift. With the stored electrical energy, it provides power to the loads when needed, thereby mitigating the risk of load curtailment during the peak hours of demand. Comparing the three subplots, it can be found that case 3 faces a more serious risk of power outages. The value of $EENS_2$ is 2.03 MW·h in case 1, 2.29 MW·h in case 2, and 3.63 MW·h in case 3. The value of $EENS$ for the system over 24 hours increases from 12.74 MW·h for case 1, 13.23 MW·h for case 2 to 16.12 MW·h for case 3. The reason for such differences is that under the conditions of case 1 and case 2, the degradation of batteries is neglected, resulting in the evaluated performance level of the BESS being higher than its actual value, and its ability to dispatch power is overestimated. In case 3, the BESS that has been in service for a certain period of time and may suffer failures is considered unable to provide the nominal performance, so severe load curtailment is more likely to occur in the power system.

TABLE IV

RELIABILITY INDICES $LOLP_m$ FOR THE THREE CASES

Node	Case 1	Case 2	Case 3
2	0.313	0.328	0.490
5	0.072	0.080	0.182
12	0.031	0.032	0.040
15	0.023	0.022	0.026
17	0.042	0.047	0.120
21	0.023	0.023	0031
26	0.025	0.025	0.025
28	0.000	0.000	0.000

Table IV presents the reliability indices $LOLP_m$ at different nodes in the above three cases. Similar to the changing trend of $EENS_m$ values, the assessment results increase when battery degradation and TR propagation are considered, especially in the areas with severe power shortage near node 2 and node 5.

The values of wind energy curtailment $\Delta W_t (1 \le t \le 24)$ are illustrated in Fig. 11. Since there is generally an incline in wind speed at night, which does not coincide with the peak loads, the wind energy curtailment reaches maximum at this time. In a power system with a high proportion of renewable energy, the BESS is introduced to compensate for the intermittent nature of wind power, thus the renewable energy accommodation capability of the system can be improved. It can be seen that the ΔW_4 value of case 1 is 4.07 MW·h, which is 4.21 MW·h in case 2, and increases to 4.90 MW·h in case 3. The daily wind energy curtailment ΔW of the power system in case 1, case 2, and case 3 is 31.36 MW·h, 33.22 MW·h, and 40.54 MW·h, respectively, illustrating that the BESS in case 3 possesses the least capacity to store the wind energy that is oversupplied. As indicated in the results, considering the impacts of battery degradation and TR propagation on the reliability of the BESS, its ability to provide services to the power system is impaired.

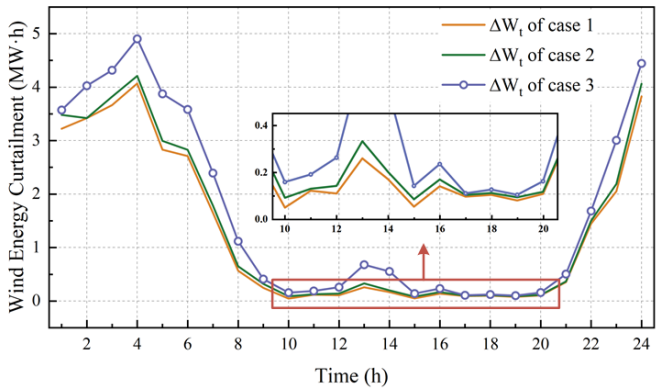

Fig. 11. Comparison of the wind energy curtailment.

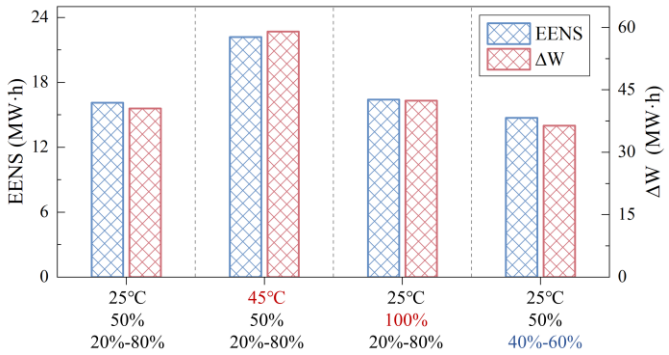

Fig. 12. Comparison of system reliability at different ambient temperature and SOC values.

C. Simulation at Different Ambient Temperatures and SOC Values

Furthermore, sensitivity analyses of temperature and SOC values are carried out. Different aging rates due to differences in ambient temperature, SOC value at idle, and SOC range during cycling are quantified, resulting in different performance levels of the BESS after a three-year operation. The system *EENS* and ΔW over the 24-hour modeling horizon at different ambient temperatures and SOC values are given in Fig. 12.

Compared to 25℃, an increase in ambient temperature impairs the reliability of the BESS due to the accelerated degradation of battery cells. Storing and cycling at different SOC values also leads to differences in the performance of the BESS. The performance reduction then results in larger values of *EENS* and ΔW, which means higher operational risk. From the results in Fig. 12, it can be concluded that operating at high temperature shortens the lifespan of the battery energy storage to a greater extent.

D. Computational performance on Larger Systems

In order to validate the effectiveness of the proposed technique on larger test systems, two additional tests involving the IEEE 118-bus system and more energy storage systems are performed. In the first test, the IEEE 118-bus system is modified, with the BESS at node 77. In the second one, two BESSs with the same structure as in previous tests are connected at node 18 and node 77, respectively.

The simulations are carried out on a computer with an Intel® Core™ i5-7400 processor (3.00GHz) and 8GB memory. The computation time of the reliability assessment based on systems with different dimensions is presented in Table V. It can be noted that the computation time of the original test (30-bus power system, a BESS with 4 battery modules) is 394.17 minutes, which becomes about 1.29 times on the 118-bus system. It also takes more time to obtain the results for the test with more battery energy storage.

In this paper, the proposed solution algorithm adopts linearization and approximation when solving the optimal scheduling model, and the TR propagation model only calculate the heat transfer of the batteries within the area affected. In this way, the computational speed is accelerated, thus achieving acceptable performance in real applications [43], [48]. In addition, advanced computing infrastructure and supercomputing mechanism can also further reduce the computation time for reliability assessment of larger systems [49].

TABLE V
COMPARISON OF COMPUTATION TIME

Test System	BESS Numbers	Computation Time (min)
30-bus system	1	394.17
118-bus system	1	509.62
118-bus system	2	770.52

VI. CONCLUSION

This paper proposes an assessment method for investigating the reliability of renewable power systems considering thermally-induced incidents of large-scale BESS. Based on the performance of each internal cell during the battery degradation process, a multi-state model of the BESS is constructed utilizing the UGF method. To accurately determine the states of battery cells, a TR propagation model of the BESS is established to extract the information on the real-time temperatures of battery cells. On this basis, the impact of grid-connected BESSs is incorporated into the reliability assessment of the power system, and a corresponding assessment framework is proposed.

The numerical results show that after the three-year operation of the grid-connected BESS, there could be a 26.5% increase in the *EENS* and a 9.18 MW·h increase in the ΔW for the 182-MW system considering thermal effects. Moreover, since the degradation process is accelerated at high temperature and some SOC ranges, resulting in a shortened lifespan of battery energy storage, the service performance of the BESS is highly related to temperature and SOC values.

Therefore, in the reliability assessment of the power system, it is necessary to consider the battery degradation and TR propagation of battery energy storage to avoid situations where the expected performance of the BESS is not achieved. In addition, further research could help the structural design and life-cycle utilization of the BESS, thereby promoting the application of battery energy storage in future power systems.

REFERENCES

[1] A. G. Olabi, M. A. Abdelkareem, T. Wilberforce, and E. T. Sayed, "Application of graphene in energy storage device – A review," *Renewable and Sustainable Energy Reviews*, vol. 135, pp. 110026, 2021.

[2] A. G. Olabi, C. Onumaegbu, T. Wilberforce, M. Ramadan, M. A. Abdelkareem, and A. H. Al – Alami, "Critical review of energy storage systems," *Energy*, vol. 214, pp. 118987, 2021.

[3] "Growth Opportunities from Decarbonisation in the Global Power Market, 2019–2030," Frost & Sullivan, San Antonio, TX, USA, 2020.

[4] F. Calero, C. A. Cañizares, and K. Bhattacharya, "Dynamic Modeling of Battery Energy Storage and Applications in Transmission Systems," *IEEE Transactions on Smart Grid*, vol. 12, no. 1, pp. 589-598, 2021.

[5] K. M. Tan, T. S. Babu, V. K. Ramachandaramurthy, P. Kasinathan, S. G. Solanki, and S. K. Raveendran, "Empowering smart grid: A comprehensive review of energy storage technology and application with renewable energy integration," *Journal of Energy Storage*, vol. 39, pp. 102591, 2021

[6] M. A. Hannan et al., "Battery energy-storage system: A review of technologies, optimization objectives, constraints, approaches, and outstanding issues," *Journal of Energy Storage*, vol. 42, p. 103023, 2021.
[7] "Renewables 2021 – Analysis and forecast to 2026," International Energy Agency, 2021.
[8] C. A. Hill, M. C. Such, D. Chen, J. Gonzalez, and W. M. Grady, "Battery Energy Storage for Enabling Integration of Distributed Solar Power Generation," *IEEE Transactions on Smart Grid*, vol. 3, no. 2, pp. 850-857, 2012.
[9] P. Denholm, J. Nunemaker, P. Gagnon, and W. Cole, "The potential for battery energy storage to provide peaking capacity in the United States," *Renewable Energy*, vol. 151, pp. 1269-1277, 2020.
[10] A. Kanchanaharuthai, V. Chankong, and K. A. Loparo, "Transient stability and voltage regulation in multimachine power systems vis-à-vis STATCOM and battery energy storage," *IEEE Transactions on Power Systems*, vol. 30, no. 5, pp. 2404-2416, 2015.
[11] P. Wang, Z. Gao and L. Bertling, "Operational Adequacy Studies of Power Systems With Wind Farms and Energy Storages," *IEEE Transactions on Power Systems*, vol. 27, no. 4, pp. 2377-2384, 2012.
[12] Z. Parvini, A. Abbaspour, M. Fotuhi-Firuzabad and M. Moeini-Aghtaie, "Operational Reliability Studies of Power Systems in the Presence of Energy Storage Systems," *IEEE Transactions on Power Systems*, vol. 33, no. 4, pp. 3691-3700, 2018.
[13] R. Sioshansi, S. H. Madaeni and P. Denholm, "A Dynamic Programming Approach to Estimate the Capacity Value of Energy Storage," *IEEE Transactions on Power Systems*, vol. 29, no. 1, pp. 395-403, 2014.
[14] C. Wang, B. Jiao, L. Guo, K. Yuan, and B. Sun, "Optimal planning of stand-alone microgrids incorporating reliability," *Journal of Modern Power Systems and Clean Energy*, vol. 2, no. 3, pp. 195-205, 2014.
[15] A. K. Onaolapo, R. P. Carpanen, D. G. Dorrell, and E. E. Ojo, "Reliability Evaluation and Financial Viability of an Electricity Power Micro-Grid System With the Incorporation of Renewable Energy Sources and Energy Storage: Case Study of KwaZulu-Natal, South Africa," *IEEE Access*, vol. 9, pp. 159908-159924, 2021.
[16] A. Perez, R. Moreno, R. Moreira, M. Orchard, and G. Strbac, "Effect of battery degradation on multi-service portfolios of energy storage," *IEEE Transactions on Sustainable Energy*, vol. 7, no. 4, pp. 1718-1729, 2016.
[17] M. Liu, W. Li, C. Wang, M. P. Polis, L. Y. Wang and J. Li, "Reliability evaluation of large scale battery energy storage systems," *IEEE Transactions on Smart Grid*, vol. 8, no. 6, pp. 2733-2743, 2017.
[18] P. Lyu et al., "Recent advances of thermal safety of lithium ion battery for energy storage," *Energy Storage Materials*, vol. 31, pp. 195-220, 2020.
[19] L. Li, C. Xu, R. Chang, et al., "Thermal-responsive, super-strong, ultrathin firewalls for quenching thermal runaway in high-energy battery modules," *Energy Storage Materials*, Vol. 40, pp.329-336, 2021.
[20] International association of fire and rescue services, Accident analysis of the Beijing lithium battery explosion which killed two firefighters[EB/OL] (2021-05-25)[2021-09-17].
[21] T. Hatchard, D. MacNeil, A. Basu, and J. R. Dahn, "Thermal model of cylindrical and prismatic lithium-ion cells," *Journal of The Electrochemical Society*, vol. 148, no. 7, p. A755, 2001.
[22] G.-H. Kim, A. Pesaran, and R. Spotnitz, "A three-dimensional thermal abuse model for lithium-ion cells," *Journal of Power Sources*, vol. 170, no. 2, pp. 476-489, 2007.
[23] S. Gao et al., "An experimental and analytical study of thermal runaway propagation in a large format lithium ion battery module with NCM pouch-cells in parallel," *International Journal of Heat and Mass Transfer*, vol. 135, pp. 93-103, 2019.
[24] X. Feng, D. Ren, X. He, and M. Ouyang, "Mitigating thermal runaway of lithium-ion batteries," *Joule*, vol. 4, no. 4, pp. 743-770, 2020.
[25] R. Sioshansi et al., "Energy-Storage Modeling: State-of-the-Art and Future Research Directions," *IEEE Transactions on Power Systems*, vol. 37, no. 2, pp. 860-875, 2022.
[26] A. M. Rei, A. M. Leite da Silva, J. L. Jardim and J. C. O. Mello, "Static and dynamic aspects in bulk power system reliability evaluations," *IEEE Transactions on Power Systems*, vol. 15, no. 1, pp. 189-195, 2000.
[27] B. Xu, "Dynamic Valuation of Battery Lifetime," *IEEE Transactions on Power Systems*, vol. 37, no. 3, pp. 2177-2186, 2022.
[28] X. Han et al., "A review on the key issues of the lithium ion battery degradation among the whole life cycle," *eTransportation*, vol. 1, pp. 100005, 2019.
[29] T. Waldmann, M. Wilka, M. Kasper, M. Fleischhammer, and M. Wohlfahrt-Mehrens, "Temperature dependent ageing mechanisms in Lithium-ion batteries–A Post-Mortem study," *Journal of Power Sources*, vol. 262, pp. 129-135, 2014.
[30] E. Redondo-Iglesias, P. Venet, S. Pelissier, "Eyring acceleration model for predicting calendar ageing of lithium-ion batteries," *Journal of Energy Storage*, vol. 13, pp. 176-183, 2017.
[31] S. Saxena, C. Hendricks, M. Pecht, "Cycle life testing and modeling of graphite/LiCoO2 cells under different state of charge ranges," *Journal of Power Sources*, vol. 327, pp. 394-400, 2016.
[32] Y. Ding, Y. Lin, and M. J. Zuo, "Multiperformance Measure Multistate Systems: General Definitions and Concepts," *IEEE Transactions on Reliability*, vol. 70, no. 1, pp. 2-12, 2019.
[33] Z. Liu, C. Tan, F. Leng, and S. Safety, "A reliability-based design concept for lithium-ion battery pack in electric vehicles," *Reliability Engineering & System Safety*, vol. 134, pp. 169-177, 2015.
[34] L. Fan, K. Wang, B. Zhang, G. Li, D. Zhai, and W. Wang, "Modeling and Simulation of Battery Energy Storage System Considering Intrinsic Inconsistency," *Automation of Electric Power Systems*, vol. 40, no. 03, pp. 110-115, 2016.
[35] S. I. Vagropoulos, A. G. Bakirtzis, "Optimal Bidding Strategy for Electric Vehicle Aggregators in Electricity Markets," *IEEE Transactions on Power Systems*, vol. 28, no. 4, pp. 4031-4041, 2013.
[36] Y. Ding, P. Wang, L. Goel, P. C. Loh, and Q. Wu, "Long-Term Reserve Expansion of Power Systems With High Wind Power Penetration Using Universal Generating Function Methods," *IEEE Transactions on Power Systems*, vol. 26, no. 2, pp. 766-774, 2011.
[37] X. Luo, Q. Zhang, H. Qi, and X. Zhang, "Lithium-ion battery thermal runaway domino effect analysis based on the CFD," *Science Technology and Engineering*, vol. 14, no. 33, pp. 327-332, 2014.
[38] M. Zhang, J. Zhang, K. Yang, H. Liu, and M. Geng, "Energy released during thermal runaway of lithium iron phosphate battery," *Chinese Journal of Power Sources*, vol. 44, no. 11, pp. 1583-1586+1621, 2020.
[39] C. F. Lopez, J. A. Jeevarajan, and P. P. Mukherjee, "Experimental Analysis of Thermal Runaway and Propagation in Lithium-Ion Battery Modules," *Journal of The Electrochemical Society*, vol. 162, no. 9, pp. A1905-A1915, 2015.
[40] P. Giorsetto and K. F. Utsurogi, "Development of a new procedure for reliability modeling of wind turbine generators," *IEEE transactions on power apparatus and systems*, no. 1, pp. 134-143, 1983.
[41] H. Pandžić, V. Bobanac, "An Accurate Charging Model of Battery Energy Storage," *IEEE Transactions on Power Systems*, vol. 34, no. 2, pp. 1416-1426, 2019.
[42] Y. Ding, A. Lisnianski, and Systems, "Fuzzy universal generating functions for multi-state system reliability assessment," *Fuzzy Sets and Systems*, vol. 159, no. 3, pp. 307-324, 2008.
[43] M. Bao, Y. Ding, C. Shao, Y. Yang and P. Wang, "Nodal Reliability Evaluation of Interdependent Gas and Power Systems Considering Cascading Effects," *IEEE Transactions on Smart Grid*, vol. 11, no. 5, pp. 4090-4104, 2020.
[44] T. Ding, R. Bo, F. Li and H. Sun, "Optimal Power Flow With the Consideration of Flexible Transmission Line Impedance," *IEEE Transactions on Power Systems*, vol. 31, no. 2, pp. 1655-1656, 2016.
[45] X. Feng, M. Ouyang, X. Liu, L. Lu, Y. Xia, and X. He, "Thermal runaway mechanism of lithium ion battery for electric vehicles: A review," *Energy Storage Materials*, vol. 10, pp. 246-267, 2018.
[46] X. Feng, "Thermal runaway initiation and propagation of Lithium-ion traction battery for electric vehicle: test, modeling and prevention," Tsinghua University, 2016.
[47] Blake D . Battery heat release data[EB/OL]. http://www.fire.tc.faa.gov. 2013-05-13.
[48] K. Morison, L.Wang and P. Kundur, "Power system security assessment," *IEEE Power and Energy Magazine*, vol. 2, no. 5, pp. 30-39, 2004.
[49] R. Billinton, N. R. Allan, *Reliability evaluation of power systems*, 2nd ed. New York, NY, USA: Plenum, 1996.

Siying Li received the B.S. degree in electrical engineering from Zhejiang University, Hangzhou, China, in 2020, where she is currently pursuing the M.S. degree in electrical engineering.

Her research interests include power system reliability and the power market.

Chengjin Ye received the B.E. and Ph.D. degrees in electrical engineering from Zhejiang University, Hangzhou, China, in 2010 and 2015, respectively. From 2015 to 2017, he served as a Distribution System Engineer with the Economics Institute, State Grid Zhejiang Electric Power Company Ltd. From 2017 to 2019, he was an assistant research fellow with the College of Electrical Engineering, Zhejiang University. Since 2020, he has been a Tenure-track Professor there.

His research interests mainly include grid resilience enhancement, as well as market mechanism and control strategy towards the integration of demand resources into power system operation.

Yi Ding (M'12) received the bachelor degree in electrical engineering from Shanghai Jiaotong University, Shanghai, China in 2000, and the Ph.D. degree in electrical engineering from Nanyang Technological University, Singapore in 2007. He is currently a Professor with the College of Electrical Engineering, Zhejiang University, Hangzhou, China.

His research interests include power systems reliability and performance analysis incorporating renewable energy resources, and engineering systems reliability modeling and optimization.

Yonghua Song (F'08) received the B.E. and Ph.D. degrees from Chengdu University of Science and Technology, Chengdu, China, and the China Electric Power Research Institute, Beijing, China, in 1984 and 1989, respectively, all in electrical engineering. He was awarded DSc by Brunel University in 2002, Honorary DEng by University of Bath in 2014 and Honorary DSc by University of Edinburgh in 2019. From 1989 to 1991, he was a Post-Doctoral Fellow at Tsinghua University, Beijing. He then held various positions at Bristol University, Bristol, U.K.; Bath University, Bath, U.K.; and John Moores University, Liverpool, U.K., from 1991 to 1996. In 1997, he was a Professor of Power Systems at Brunel University, where he was a Pro-Vice Chancellor for Graduate Studies since 2004. In 2007, he took up a Pro-Vice Chancellorship and Professorship of Electrical Engineering at the University of Liverpool, Liverpool. In 2009, he joined Tsinghua University as a Professor of Electrical Engineering and an Assistant President and the Deputy Director of the Laboratory of Low-Carbon Energy. During 2012 to 2017, he worked as the Executive Vice President of Zhejiang University, as well as Founding Dean of the International Campus and Professor of Electrical Engineering and Higher Education of the University. Since 2018, he became Rector of the University of Macau and the director of the State Key Laboratory of Internet of Things for Smart City.

His current research interests include smart grid, electricity economics, and operation and control of power systems. Prof. Song was elected as the Vice-President of Chinese Society for Electrical Engineering (CSEE) and appointed as the Chairman of the International Affairs Committee of the CSEE in 2009. In 2004, he was elected as a Fellow of the Royal Academy of Engineering, U.K. In 2019, he was elected as a Foreign Member of the Academia Europaea.

Minglei Bao received the B.S. degree in electrical engineering from Shandong University and the Ph. D degree in electrical engineering from Zhejiang University in 2016 and 2021, respectively. He is currently a postdoctor at Zhejiang University, Zhejiang, China.

His research interests include reliability analysis of the integrated energy system, complex network and the power market.